

Influence of Plasma Spray Parameters on the Cracking Behavior of Yttria Stabilized Zirconia Coatings

A. Kucuk, C.G. Dambra, and C.C. Berndt

(Submitted 30 October 2000; in revised form 10 November 2000)

Thermal spray coatings enhance the material properties of substrates but this attribute may be negated if the coatings themselves fail. This paper investigates the performance of an important family of coatings as one step in improving the resistance of the coating/substrate system to mechanical failure.

Thermal barrier coatings of yttria partially stabilized zirconia (YSZ) with a NiCrAlY bond coat were air plasma sprayed onto mild-steel substrates. The spray process parameters were varied according to top and bond coat thickness, stand off distance, and substrate temperature. These 17 groups of coating types, with six identical samples in each group, were four point bend tested while coupled with an *in-situ* acoustic emission transducer. Optical microscopy was then used to examine and map the resulting crack patterns. Measurements of the number of cracks, crack separation, delaminating length, and micro-crack density were also made. The combination of this information, along with properties obtained from the four point bend tests and acoustic emission signals, provided insight into the cracking and delaminating processes.

Keywords: acoustic emission, cracking behavior, four-point bending, thermal barrier coatings, zirconia

1. Introduction

Plasma sprayed duplex NiCrAlY/YSZ thermal barrier coatings (TBCs) have been widely used in power generation and aviation as protective coatings for underlying metallic parts.^[1] Although the thermal and high temperature corrosion resistance of these coatings improve the engine efficiency, poor mechanical properties and reliability still present in-service problems. Therefore, a better understanding of deformation and cracking in these coatings is necessary for improved reliability and enhanced coating designs.

Few studies of the deformation characteristics and cracking behavior of thermally sprayed materials have been reported in the open literature. Berndt and his co-workers^[2-4] have extensively studied mechanical properties, failure mechanisms, and cracking properties of thermally sprayed oxide coatings including alumina, alumina-titania, and zirconia-yttria under thermal cyclic, indentation, three and four point loading, and tensile adhesion loading stresses over the last 20 years. They have reported that the properties of coatings strongly depend on the complex microstructure consisting of anisotropic splats, voids, and micro- and macro-cracks retained under process residual stresses. In essence, these prior studies have concluded that thermal spray materials can be treated as composites that are heavily influenced by porosity. Additionally,

the nature of the thermal spray process gives rise to certain orientations of micro- and macro-cracks that confer the ultimate mechanical response of the coating/substrate system. Acoustic emission and appropriate statistical analysis were also used to assess the cracking processes, in real time, so that the cracking propensity could be related to the processing conditions.

Colin et al.^[5] examined plasma sprayed magnesium zirconate (MZ) and chromium oxide (CO) coatings using double cantilever beam and four point bend tests. With the aid of acoustic emission (AE) and optical microscopy, they found a correlation between damage mechanisms, coating toughness, and the acoustic emission response of the coatings. Brown and Turner^[6] studied plasma sprayed hydroxyapatite coatings using four point tests coupled with AE, and optical/electron microscopy. They found that the AE count rate during the four point bend tests depended on the process-induced residual stresses. Voyer et al.^[7] also utilized *in-situ* AE analysis and microscopy to study cracking of YSZ coatings during thermal cycle tests, and Schmidt et al.^[8] studied creep damage behavior of thermal barrier coatings.

However, additional studies of the damage and damage detection in thermally sprayed materials are needed. The present study summarizes the cracking behavior of large numbers of plasma sprayed TBCs under biaxial stresses. *In-situ* AE analysis and post-

A. Kucuk, C.G. Dambra, and C.C. Berndt, Department of Materials Science and Engineering, State University of New York at Stony Brook, 306 Old Engineering, Stony Brook, NY 11794-2275. Contact e-mail: cberndt@notes.cc.sunysb.edu.

test microscopy were used to investigate the cracking sequence and damage mechanisms.

2. Experimental Procedure

2.1 Sample Preparation

A top coat of commercially available 8 wt.% yttria stabilized zirconia (YSZ) and a bond coat of NiCrAlY was air plasma sprayed onto mild-carbon steel substrates (90 × 26.5 × 2.6mm). The spray parameters were altered according to 1) top-coat thickness (300 or 500µm), 2) bond-coat thickness (100 or 250µm), 3) stand-off distance (80 or 100mm), and 4) the substrate pre-heated temperature (273 or 393 K).

The substrates were grit blasted to an average roughness of 4.0 ± 0.5µm. Each sample was then cleaned with ethyl alcohol. A handheld infrared temperature detector was used to measure the pre-heat temperature of the substrate prior to spraying. The coatings were sprayed to dimensions of 30 × 26.5mm, leaving bare substrate on each side of the coating. Each substrate was air cooled on the back-

side to avoid overheating during spraying.

A plasma torch, mounted on a six-axis articulated robot, was used to spray 17 groups of coating types. Each group contained six samples, which are listed in Table 1. The spray parameters used during the spraying of the top and bond coatings are listed in Table 2.

2.2 Four Point Bend Testing and Acoustic Emission Analysis

Four point bend tests were performed using a universal (tension/compression) test machine. The lengths of the inner and outer spans of the testing rig were 20 and 40mm, respectively. The testing was performed at a constant crosshead displacement rate of 10µm/sec. All of the 102 coatings were tested in tension during bending. Additional information about the four point bend testing has been previously presented.^[9] During the four-point bend testing, AE signals were received with the use of a transducer placed on a non-coated section of the steel substrate. The AE analysis techniques are summarized in Kucuk et al.^[10]

Table 1 Samples sprayed according to experimental design

Sample Designation	Bond Coat (µm)	Top Coat (µm)	Substrate Temperature (K)	Stand Off Distance (mm)
S1	100	300	393	80
S2	100	300	393	100
S3	250	300	393	80
S4	250	500	393	100
S5	250	500	393	80
S6	100	500	273	80
S7	100	500	273	100
S8	250	300	273	80
S9	100	500	393	80
S10	100	300	273	80
S11	250	300	393	100
S12	250	300	273	100
S13	250	500	273	80
S14	250	500	273	100
S15	100	300	273	100
S16	100	500	393	100
S17	175	400	333	90

2.3 Analysis of Macro-Cracking Behavior

One sample from each of the 17 groups was then randomly selected for further examination. These chosen samples were mounted in epoxy resin and vacuum impregnated. The samples were cut with an abrasive saw in the tensile strain direction such that the cross-section was perpendicular to the loading and support beams. The cross-sections were polished using conventional methods and examined with a reflected light microscope. This allowed for the macroscopic cracks in the zirconia top coat and NiCrAlY bond coat to be counted and mapped. Delamination of the top-coat from the bond-coat and of the bond-coat from the substrate were also mapped. Average crack separation and length of delamination were measured using image analysis techniques.

2.4 Analysis of Micro-Cracking Behavior

The polished samples were examined at greater magnifications (200-500×) to allow for the quantitative analysis of the microcracks that formed during testing. The Linear Intercept method of the ASTM E 112 "Standard Test Methods for Determining Average Grain Size"^[11] was modified to measure average crack separation. This method involved the counting of micro-cracks in three separate coating directions; i.e., directions that are parallel, transverse, and at 45° to the direction of strain. Lines of known length were drawn at random positions on the cross-sectional coating micrographs. The number of micro-cracks that intercepted the line was determined. Three measurements, in each of the three directions, were made. Micro-crack density was then determined by dividing the number of cracks by the length of the test line. For this method, micrographs of the center of the coating

length were used. This ensured that any effects arising from the support bars were eliminated.

3. Results

3.1 Four Point Bending

The bending yield stress (σ_{YB}) and bending modulus (E_B) calculated from the load-displacement data are summarized in Table 3. Details of the four point bend test methodology have been reported previously.^[9]

3.2 Acoustic Emission (AE)

The results of the AE analysis are summarized in Table 3. The number of acoustic events and the cumulative AE energies were obtained throughout the bend test. The data were separated into elastic and plastic regions using the AE analysis described in Kucuk et al.^[12] The samples were grouped into categories according to their respective AE activity output (Fig. 1). In general, those coatings that exhibited delamination, showed the larger amount of AE activity and released higher quantities of energy during the testing. These coatings were thicker and sprayed at a closer distance onto a pre-heated substrate.

3.3 Macro-Cracking Analysis

Further analysis was performed on the polished coating cross-sections. In this case, microscopy allowed for detailed observation of the cracks in both the top and bond coats. Maps of the cracking patterns were generated for each of the coating samples (Fig. 2). During this analysis procedure, cracks in both the top and bond coats were counted. Crack length and total delamination length were also deter-

Table 2 Spray parameters for the coating system

	YSZ	NiCrAlY
Torch Type	Metco 3MB	Metco 3MB
Nozzle	Metco G H	Metco G H
Current (A)	600	500
Voltage (V)	70	70
Primary Gas, Ar (l/min)	40	40
Secondary Gas, H ₂ (Ymin)	11	8
Powder Carrier Gas, N ₂ (Ymin)	3.5	3.65

mined. Finally, average crack separation (i.e., average distance between the vertical cracks) was measured. The measurements and observations were made from micrographs and are summarized in Table 4.

It was observed that coatings either exhibited a well-distributed cracking pattern across the entire coating surface (i.e., sample S1), or the cracking was localized to the support beams of the testing fixture (i.e., sample S14); see Fig. 2. The number of cracks that were found in the zirconia top-coat varied from 3 to 30, while the number varied from 7 to 34 in the bond-coat. Delamination of the ceramic top-coat, often considered to be catastrophic failure, was observed in some samples (i.e., samples S4 and S9). This delamination was often found to occur slightly above the ceramic/bond coat interface (Fig. 3). This observation is consistent with the process of delamination occurring by the propagation of the horizontal crack through the ceramic layer, near the interface with the bond-coat. This phenomenon indicates that the adhesion between the top and bond coats was high. In some instances, minimal delamination of

the bond-coat from the substrate was also found (i.e., samples S5 and S13).

3.4 Micro-Cracking Analysis

Although measurements of crack density are reported for three directions, any future reference to micro-crack density refers to the measurement made in the direction parallel to the stress/strain axis. This direction was chosen because the most likely direction of crack propagation is perpendicular to the stress axis. Micro-crack density is reported in Table 4. However, the test-induced crack density may have overestimated the extent of cracking because it is difficult to distinguish between micro-cracks and splat boundaries. Furthermore, micro-cracks that formed as a result of processing, prior to testing, were also counted.

4. Discussion

4.1 Cracking Sequences and Mechanisms

The optical micrographs taken of the coating cross-sections aided in the mapping (Fig. 2) and

Table 3 Summary of AE events observed during the four point bend test along with the average bending yield stress and modulus value for each group (“a.u.” indicates arbitrary units).

Sample	$N_{AE} \times 10^{-3}$ Elastic	$E_{AE} \times 10^{-3}$		$N_{AE} \times 10^{-3}$ Total	$E_{AE} \times 10^{-3}$ Total (a.u.)	σ_{YB} (MPa)	E_B (GPa)
		Elastic (a.u.)					
S1	1.1±0.4	0.6±0.4		2.521.2	1.9±0.9	301223	114211
S2	2.820.8	3.922.2		10.1±1.4	1222	260226	89211
S3	4.720.5	3.822.2		19.6±4.4	52224	92238	29±14
S4	1.920.7	1.121.0		16.222.4	76±20	14218	4±4
S5	4.221.6	5.822.8		20.9±5.0	40±17	225±41	72217
S6	1.6±0.3	2.120.3		11.3±1.0	16±3	160253	51219
S7	2.820.8	3.6±1.7		10.121.4	1222	260226	89±11
S8	2.220.7	1.5±0.7		8.625.1	522	328±43	11427
S9	2.7±0.5	4.6±1.7		22.02 6.7	52±23	62243	21214
S10	2.7±0.8	3.4±1.9		12.3±2.0	15±3	206288	78236
S11	1.821.5	1.8±1.7		4.121.6	623.8	27±50	8±14
S12	1.120.3	0.7±0.5		2.921.1	3.7±2.5	73299	21229
S13	3.621.2	4.1±2.4		16.5±2.8	21±8	250230	86215
S14	1.820.7	1.020.5		11.4±2.7	42±14	1±25	1±6
S15	0.44±0.06	0.4920.06		0.9520.15	1.2±0.3	440±61	171±17
S16	0.820.4	1.1±0.5		2.8±0.9	2.9±1.1	371259	144219
S17	1.0±0.3	0.720.6		11.7±4.9	30220	11±44	4±13

**Table 4 Summary of the data collected and the observations made during this study:
A brief description of the cracking behavior is also given.**

	Top Coat N	d(μm)	Bond Coat d(mm)	N	Crack Density per mm	Delamination (μm)	Comments
S1	30	530 ± 183	394 ± 249	34	76	0	Cracking well distributed, high relative strength, no delamination
S2	R: 7 L: 6	867 ± 296	373 ± 180	R: 14 L: 18	89	68	Localized cracking, delamination of top and bond coats
S3	R: 9 L: 7	537 ± 318	390 ± 249	R: 8 L: 6	45	300	Localized cracking, delamination of top and bond coats, irregular crack pattern
S4	8	2216 ± 476	894 ± 517	R: 4 L: 9	43	1300	Cracking is distributed, severe delamination of top coat, large average crack separation
S5	R: 7 L: 5	942 ± 363	666 ± 237	R: 7 L: 9	29	800	Localized cracking, severe delamination of top and bond coats
S6	R: 8 L: 5	1135 ± 527	680 ± 178	R: 10 L: 3	27	390	Localized cracking, delamination of top coat
S7	R: 5 L: 3	545 ± 429	314 ± 78	R: 6 L: 11	26	600	Localized cracking, severe delamination of top coat
S8	R: 3 L: 5	766 ± 262	395 ± 115	R: 2 L: 6	44	60	Localized cracking, delamination of bond coat, good adhesion at top/bond coat interface
S9	R: 3 L: 4	793 ± 534	328 ± 73	R: 8 L: 13	41	1093	Localized crackling, large thru-cracks, major delamination of top coat at both supports
S10	R: 3 L: 6	1004 ± 85	443 ± 148	R: 5 L: 9	42	259	Localized cracking, beginnings of delamination in top coat at one support
S11	R: 4 L: 3	1448 ± 107	612 ± 82	R: 3 L: 4	44	0	Localized crackling, start of branching at bond coat suggesting delamination about to occur
S12	R: 2 L: 4	663 ± 504	729 ± 145	R: 3 L: 4	42	225	Localized cracking, delamination of top and bond coat both at the same support
S13	R: 4 L: 6	733 ± 153	749 ± 134	R: 4 L: 6	37	0	Localized cracking, delamination of bond coat only suggesting better adhesion between top and bond coat
S14	R: 2 L: 1	464	459 ± 114	R: 5 L: 6	46	428	Localized cracking, large thru-cracks, delamination of top coat, least amount of cracks
S15	R: 19 L: 8	535 ± 165	465 ± 88	R: 13 L: 4	60	0	Crackling relatively distributed, strongest sample in group, least amount of AE activity
S16	R: 5 L: 9	702 ± 160	745 ± 205	R: 3 L: 5	48	0	Localized cracking, no delamination
S17	R: 5 L: 9	979 ± 511	641 ± 395	R: 6 L: 10	49	100	Localized cracking, delamination of top coat

*N = the number of vertical cracks observed. R:L = the right and/or left side of the coating cross-section. d = the average crack separation.

explanation of the cracking sequence through the coatings. It was observed that the cracking began at the surface of the ceramic top-coat where the stresses generated by the four-point bend test are the greatest. The cracks propagated downward through the coating in a vertical direction (i.e., propagating from the outside surface of the TBC toward the substrate). Vertical macro-cracks were found to be either well-distributed throughout the coating length, or, more often, localized at the support beams of the testing fixture. Cracks will first generate near this region because the coating strain may have been slightly higher near the support bars.^[13] These vertical cracks often propagated through individual splats rather than passing through splat boundaries (Fig. 4).

Once propagation through the top-coat was completed, the vertical cracks either 1) continued on as vertical cracks through the bond-coat, or 2) were deflected horizontally in the top-coat in the region near the top-coat/bond-coat interface, to form a delamination. In the first case, the cracks passed through splat boundaries of the bond-coat, sometimes leading to localized delamination of the bond-coat from the substrate (e.g. samples S3 and S13). In the second case, often considered catastrophic failure of the coating, delamination, in effect, separated the top-coat from the rest of the coating system. This separation relieved the strain energy stored in the ceramic coating near the area that delaminated. However, vertical cracking of the bond-coat continued and sometimes led to delamination of the bond-coat as well.

Cracking and delamination result from the build-up of strain energy within the coating system. The amount of strain energy stored in the coating during the bend tests is proportional to the strength of the coating. This stored energy can be decreased by the formation of cracks in the coating.^[14] This is observed in samples S1 and S15, the strongest samples of the group. These coatings also exhibited the largest number of vertical segmentations and no delamination, indicating high adhesion between layers. It has been found that vertical segmentations can indeed help

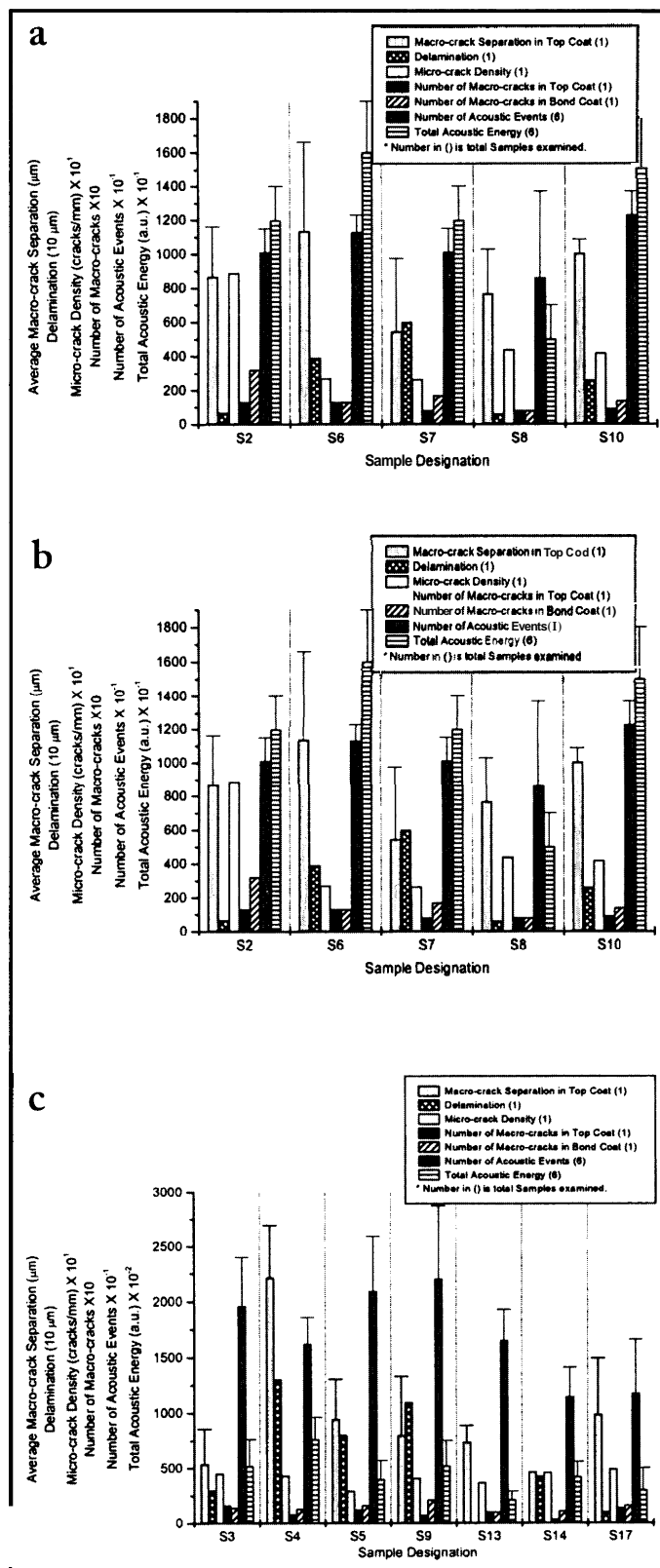


Fig. 1 Comparisons of cracking behavior and AE responses of the coatings during the four point bend tests. Samples were categorized according to (a) "low," (b) "medium," and (c) "high" groups depending on their cumulative AE energy released during the tests. Note the differences in scaling.

prevent coating delamination mechanisms and greatly improve their lifespans.^[15] This mode of cracking accommodates for the buildup of strain in the coating without the occurrence of catastrophic failure. Those coatings, which were sprayed with thicker top and bond coats, were found to be more susceptible to delamination and yielded fewer vertical cracks (e.g. samples S4, S9, and S14).

The relation between macro-crack separation and bending yield stress is shown in Fig. 5. Macro-crack separation was calculated by measuring the average distance between vertical macro-cracks. If the cracking was localized at the support beams, the large distance between the two groupings was not taken into account. This graph illustrates how an increase in crack separation causes a decrease in the bending yield stress of the coating system.

Andritschky et. al.^[16] reported that coatings relax close to the cracks as they form, creating a stress distribution. They developed an analytical equation

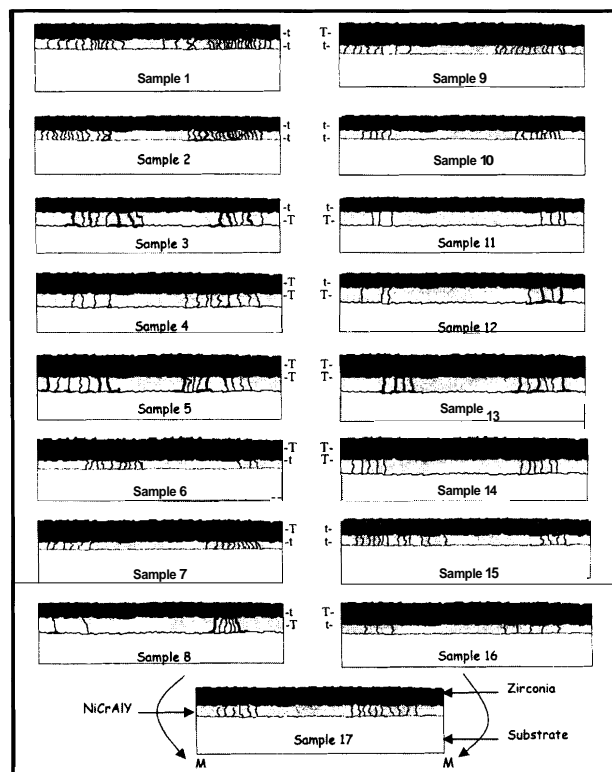


Fig. 2 Maps of cracking behavior as observed after four point bend tests. Sketches represent cross-sections taken at a direction that is parallel to that of strain. M refers to the moment direction during testing. Pictures are of entire coating length and include zirconia top coat, NiCrAlY bond coat, and mild-steel substrate. T = (thick) 250 or 500 μm for bond and top coat, respectively. t = (thin) 100 or 300 μm for bond and top coat, respectively.

to support this trend. It was observed that after cracking, the stress within the coating is much lower than the fracture resistance. Therefore, further cracking will require a significant increase in the applied stress. An explanation for the high yield stress, in samples S1 and S15 for example, can be that the cracks formed towards the end of the four point test, resulting in more stress available for crack formation. Thus, when a crack was initiated during this period of high stress, there was not likely to be sufficient stress relief. The prime mechanism for relief of this stress would be further cracking in the vicinity of the pre-existing crack. Therefore, in other words, the stress relief caused by the initial crack spawns a localized family of similar cracks so that the overall macro-crack separation is decreased.

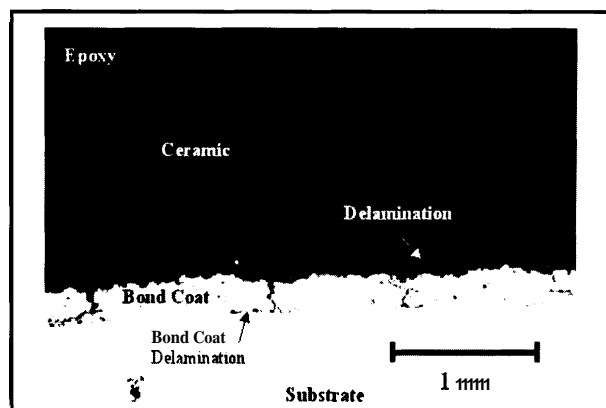


Fig. 3 Optical micrograph of coating cross-section parallel to direction of strain. Micrograph shows evidence of vertical macro-cracks, top coat delamination, bond coat cracking, and bond coat delamination. Image taken at 50X magnification

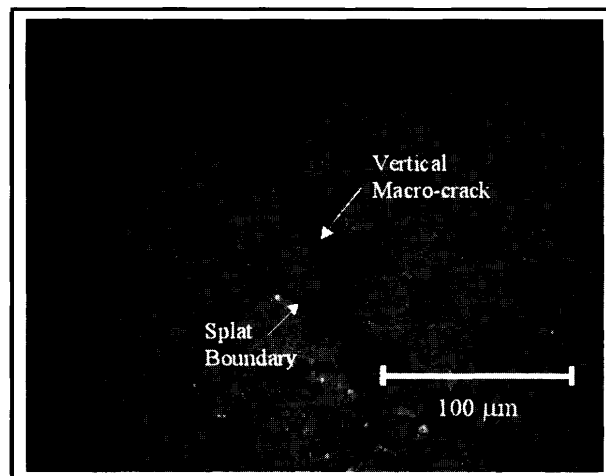


Fig. 4 Micrograph showing vertical macro-crack passing through individual splats. Image taken at 500X magnification

It can be noted that there is a discrepancy in some of the data points in Fig. 5 (e.g. samples S3, S9 and S14). An explanation for their deviation from the exponential trend is the fact that they exhibited a large amount of delamination as a result of deformation. This large amount of delamination accounts for the larger release of strain energy in these coatings. Furthermore, micro-cracking behavior is not clear at this point, and a mechanism was not suggested.

4.2 Acoustic Emission vs. Cracking

As mentioned above, the AE response of the coatings during four point bend tests was primarily dominated by delamination, secondarily by the vertical macro-cracks, and finally by the micro-cracks. It can be seen in Fig. 1 that the samples in the "low" category exhibited almost no delamination; whereas the samples in the "high" category severely delaminated. It was not surprising that the delamination generated more AE energy when the microstructure of the thermal spray coating was considered. The thermal spray coatings evolve from cohered splats, which form from the spreading of molten/semi-molten particles on the substrate (or underlying layer) at a high impact velocity.^[1] The cohesion between splats in the direction perpendicular to the spray direction is better than the cohesion in the direction parallel to the spray direction. This would be expected because both the mechanical anchoring and the chemical binding between splats, and the total contact area per two splats, are higher in the perpendicular direction. The hardness measurements carried out on the top surface

and cross-sectional areas showed that the cross-sectional hardness was higher; thereby indicating that the cohesion was enhanced in the direction perpendicular to spray direction.^[17] Therefore, delamination would require more energy and generate a higher AE response. Voyer et al.^[7] also reported that top coat delamination, which occurred during thermal cycling of TBCs, generated a larger number of AE signals than reported for vertical cracks.

To compare the AE responses of the coatings during the tests with the cracking behavior, a unique parameter, which would quantify the cracking behavior and take delamination, vertical macro-cracks, and micro-cracks into consideration, needed to be developed. A parameter called "total macro-crack length (TML)" would serve this purpose. The TML was the summation of the total delamination length and the total vertical macro-crack length, in both the top and bond coats, within the examined cross-sectional plane. Note that delamination and macro-cracks were weighed equally, and micro-cracks were not included in this value since it was not possible to determine the weight fraction for different crack types. In addition, it was assumed in the TML calculations that delamination and vertical cracks propagated throughout the entire coating width, which was not necessarily true. One may be able to use fracture toughness values in different directions to estimate the weight fraction of the various types of cracks. Similarly, gradual layer removal throughout the width would provide better information regarding the length of the crack in this direction. Nevertheless, the aforementioned assumptions were adequate for the current explor-

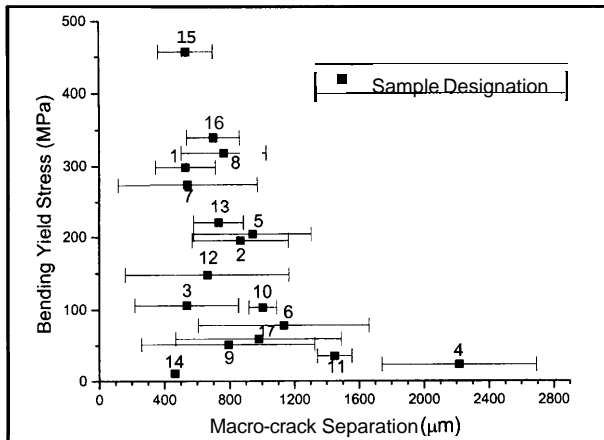


Fig. 5 Comparison of the **bending yield stress** of the coating samples with the average macro-crack separation measured **after** deformation.

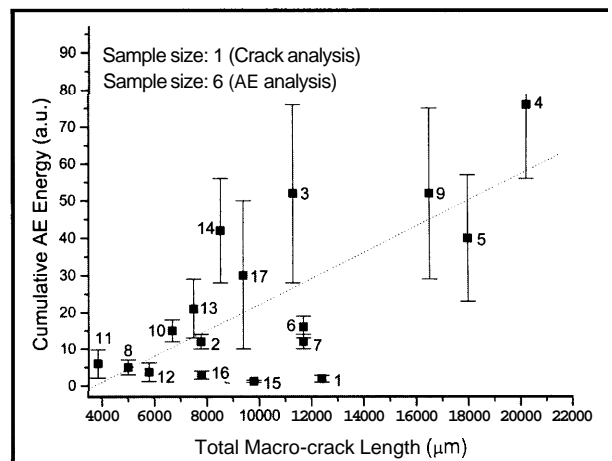


Fig. 6 Change of cumulative AE energy with total macro-crack length (TML)

atory study and complex issues regarding the exact crack nature will be studied in the future.

Figure 6 illustrates the change of cumulative AE energy with TML. As seen, the cumulative AE energy increases with increasing TML within the experimental variations. Samples with no delamination but with several vertical macro-cracks, such as samples S1, S15, and S16, slightly deviated from the linear trend, indicating another weakness in the TML calculations. It was noticed that the coatings that yielded cracks with larger opening displacement (i.e., larger crack widths), such as samples S4 and S14, generated higher AE responses than those with smaller openings, such as samples S15 and S16.

In Fig. 7, the change of average AE energy with the cumulative energy per unit length of TML is presented. Strikingly, the slope is close to one for a linear trend. Further study of this issue is necessary. It is believed that the AE energy may be used to determine the fracture toughness of the coating showing the correlation suggested in Fig. 7.

A simple relationship between AE response and micro-cracking has not yet been found. This could be because 1) macro-cracks play such a dominant role in AE response that the influence of micro-cracking was overshadowed, or 2) the method employed to quantify micro-cracking during this study was not an accurate and reliable one.

4.3 Influence of Spray Parameters on Failure

As indicated above, the coatings with thick top coat layers were more susceptible to macro-cracking,

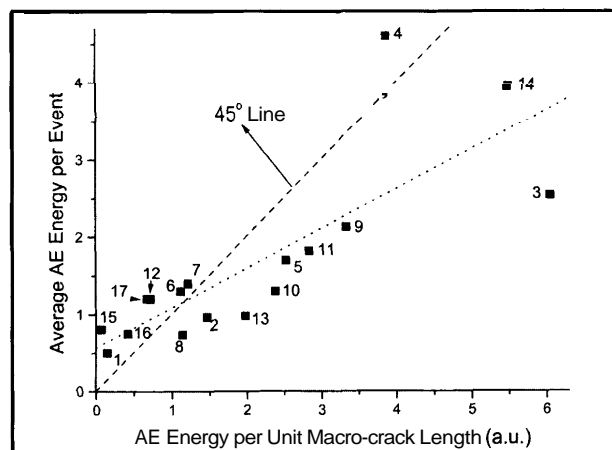


Fig. 7 Change of average AE energy with the AE energy per unit total micro-crack length (TML). Note the linear trend with a slope close to 45°.

as can be easily distinguished from the micrographs. A statistical analysis confirmed that both vertical crack length and delamination amount (and, in turn, TML) increased with increasing top coat thickness and substrate temperature within the studied range. However, no influence from bond coat thickness on TML was significantly noticed. The statistical analysis also showed that increasing stand off distance could decrease the TML at a relatively poor confidence level of less than 70%. Although such a low level of confidence in the influence of the stand off distance obscures the firm conclusions of such a trend, it is clear that relationships of such a nature exist.

Previously, we found that the yield strength of these same coatings decreases with increasing top coat thickness and the substrate temperature.^[9] Similarly, coatings with thicker top and bond coats sprayed on pre-heated substrates at a short standoff distance exhibited a higher number of AE events with higher AE energy.^[12] As a result, cracking behavior, strength of the coating, and AE response under deformation showed similar indications of a microstructure that built-up uniquely depending on the spray parameters.

The effects of process parameters, which were examined in the current study, on the strength and AE response of the coatings under loading were previously discussed in detail.^[9,12] Briefly, it was suggested that the process residual stresses played a critical role in the deformation characteristics of the coatings. It was suggested, for instance, that thicker top coat layers would result in higher residual stress levels as a result of broad temperature distributions, going from top to bottom, throughout the large coating thickness. Similarly, Levit et al.^[18] reported that residual stresses in the top coat layer were compressive in nature for the coatings sprayed on a pre-heated substrate as a result of the mismatch in coefficient of the thermal expansions (CTE) of ceramic and metallic layers. One would expect that the presence of such compressive stresses would make the top coats less susceptible to cracking.

However, one should also consider the stress built-up at the top coat/bond coat interface that could promote separation of these two layers (i.e., delamination). On the contrary, none of the delamination was observed at the exact top coat/ bond coat interface, but in the top coat near the interface. This phenomenon is commonly observed. Miller and

Lowell^[19] observed this failure near the top/bond coat interface in their thermal cycle tests. They also found that cooling stresses are responsible for failure by delamination. This delamination in the top coat, near the interface, could arise because of the mechanical interlocking resulting from the rough surface of the bond coat.

5. Conclusion

Plasma sprayed thermal barrier coatings, with varied processing parameters, were tested using a four point bend test arrangement while coupled with an *in-situ* acoustic emission monitoring system. Post-examination of the resulting crack patterns and behavior was carried out using optical microscopy. It was observed that a series of parallel cracks (perpendicular to the direction of strain) formed, which were either localized at the support bars of the four point test rig or well distributed throughout the length of the coating. Similar cracks were also present in the bond coating. Horizontal delamination of the top coat, and bond coat in some instances, occurred in samples with thicker coatings. This delamination occurred in the top coat near, but not exactly at, the top/bond coat interface. Delamination resulted in a higher AE energy output during the testing.

Those coatings that exhibited a well-distributed cracking pattern were found to have higher yield strength and bending modulus. These coatings were also found to have a thinner bond coat and were sprayed onto a cooler substrate. Furthermore, the influence of micro-crack density on the overall mechanical properties of the coating samples used in this study was not clearly understood.

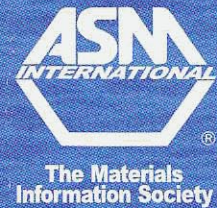
Acknowledgments

This research was funded by NSFMRSEC DMR grant number 9632570 and ONR grant number N00014-97-0843. One of the authors (C. Dambra) would like to thank the URECA Summer Fellowship Program at SUNY at Stony Brook for financial support. The assistance in sample preparation by Rogerio S. Lima, SUNY Stony Brook,

was greatly appreciated. Thanks also go to Dr. Ufuk Senturk, SUNY Stony Brook, for his stimulating discussion in some analyses.

References

1. L. Pawlowski: *The Science and Engineering of Thermal Spray Coating*, John Wiley & Sons, New York, NY, 1995.
2. R.A. Miller and C.C. Berndt: *Thin Solid Films*, 1984, vol. 119, pp. 195-202.
3. C.K. Lin and C.C. Berndt: *J. Mater. Sci.*, 1995, vol. 30, pp. 111-117.
4. C.C. Berndt: *J. Mater. Sci.*, 1989, vol. 24, pp. 3511-3520.
5. C. Colin, M. Boussuge, and D. Valentin: *J. Mater. Sci.*, 1988, vol. 23, pp. 2121-2128.
6. I.G. Turner and S.R. Brown: *Surf. Eng.*, 1998, vol. 14, pp. 309-313.
7. J. Voyer, F. Gitzhofer, and M.I. Boulos: *J. Thermal Spray Technol.*, 1998, vol. 7, pp. 181-190.
8. U.T. Schmidt, O. Vohringer, and D. Lohe: *Tran. ASME*, 1999, vol. 121, pp. 678-682.
9. A. Kucuk, C.C. Berndt, U. Senturk, R.S. Lima, and C.R.C. Lima: *Mater. Sci. Eng. A*, 2000, vol. 284, pp. 29-40.
10. A. Kucuk, R.S. Lima, and C.C. Berndt: *J. Am. Ceram. Soc.*, 2001, accepted for publication.
11. *Annual Book of ASTM Standards*, American Society for Testing and Materials, Philadelphia, PA, 1992, vol. 3.03, pp. 55-71.
12. A. Kucuk, C.C. Berndt, U. Senturk, and R.S. Lima: *Mater. Sci. Eng. A*, 2000, vol. 284, pp. 41-50.
13. U. Wiklund, P. Hedenqvist, and S. Hogmark: *Surf. Coat. Technol.*, 1997, vol. 97, pp. 773-778.
14. H.L. Tsai and P.C. Tsai: *J. Mater. Eng. Perform.*, 1995, vol. 4, pp. 689-696.
15. S. Stecura: *Thin Solid Films*, 1989, vol. 182, p. 121-139.
16. M. Andritschky, P. Alpuim, D. Stover, and C. Funke: *Mater. Sci. Eng. A*, 1999, vol. 271, pp. 62-69.
17. R.S. Lima, U. Senturk, C.C. Berndt, and C.R.C. Lima: paper presented at United Thermal Spray Conference, Dusseldorf, Germany, 17-19 March 1999.
18. M. Levit, I. Grimberg, and B.Z. Weiss: *Mater. Sci. Eng. A*, 1996, vol. 206, pp. 30-38.
19. R.A. Miller and C.E. Lowell: *Thin Solid Films*, 1982, vol. 95, pp. 265-273.



practical FAILURE ANALYSIS

*Overtorque
in Bolts*

*Failure Analysis
at NTSB*

*Performance of
PH 13-8 Mo Stainless
Helicopter Components*

In cooperation with:



International
Metallographic
Society, Inc.
An Affiliate Society of ASM International

*Volume 1
Issue 1
February 2001*